

Spin liquid state in an emergent honeycomb lattice antiferromagnet

J. Khatua,¹ D. Tay,² T. Shiroka,^{2,3} M. Pregelj,^{4,5} K. Kargeti,⁶ S. K. Panda,⁶ G. B. G. Stenning,⁷ D. T. Adroja,^{7,8} and P. Khuntia^{1,9,*}

¹*Department of Physics, Indian Institute of Technology Madras, Chennai 600036, India*

²*Laboratorium für Festkörperphysik, ETH Zürich, CH-8093 Zurich, Switzerland*

³*Center for Neutron and Muon Sciences, Paul Scherrer Institut, CH-5232 Villigen PSI, Switzerland*

⁴*Jožef Stefan Institute, Jamova cesta 39, 1000 Ljubljana, Slovenia*

⁵*Faculty of Mathematics and Physics, University of Ljubljana, Jadranska u. 19, 1000 Ljubljana, Slovenia*

⁶*Department of Physics, Bennett University, Greater Noida, Uttar Pradesh 201310, India*

⁷*ISIS Facility, Rutherford Appleton Laboratory, Chilton, Didcot, Oxon OX11 0QX, United Kingdom*

⁸*Highly Correlated Matter Research Group, Physics Department, University of Johannesburg, Auckland Park 2006, South Africa*

⁹*Quantum Centre of Excellence for Diamond and Emergent Materials, Indian Institute of Technology Madras, Chennai 600036, India*

(Dated: July 9, 2024)

In rare-earth based frustrated magnets, the synergistic interplay between spin correlations, spin-orbit coupling, and competing exchange interactions provides a promising route to realize exotic quantum states with nontrivial excitations. Here, through thermodynamic and local-probe measurements down to 16 mK, we demonstrate the exotic magnetism and spin dynamics in the nearly perfect emergent honeycomb lattice antiferromagnet TbBO₃. The latter embodies a frustrated lattice with a superimposed triangular lattice, constituted by additional Tb³⁺ ions at the center of each hexagon. Thermodynamic experiments reveal the presence of dominant antiferromagnetic interactions with no indications of either long-range order or spin freezing down to 50 mK. Despite sizable antiferromagnetic exchange interactions between the Tb³⁺ moments, muon-spin relaxation does not detect any signatures of long-range magnetic order or spin-freezing down to 16 mK. This suggests that the spin-orbit driven anisotropic exchange interaction engender a strong frustration, crucial to induce a persistent spin dynamics. The specific-heat data exhibit a $T^{2.2}$ power-law behavior at low temperatures, suggesting gapless excitations consistent with theoretical predictions. The scaling of muon relaxation rate as a function of the characteristic energy scale for several spin-liquid candidates, including TbBO₃, demonstrates a thermally activated behavior. This is consistent with NMR results on TbBO₃ and reminiscent of a universal QSL behavior, here attributed to short-range spin correlations. Our experimental results are supported by density functional theory + Hubbard U and crystal electric-field calculations, which propose TbBO₃ as a promising platform to realize the theoretically proposed quantum disorder state in an anisotropy-driven frustrated honeycomb lattice.

Quantum materials with geometrical frustration and competing degrees of freedom can have highly degenerate ground states, exhibiting rich many-body quantum phenomena. The latter have triggered interests not only in fundamental condensed-matter research, but also as key ingredients for realizing robust quantum-computing technologies [1–3]. To date, the most sought-after challenge is the experimental realization of the quantum spin liquid (QSL) state. This is an elusive state of matter which, despite strong magnetic interactions, is characterized by the absence of a long-range magnetic order even at absolute zero [2, 4–6]. QSL is a highly entangled state, often intricately associated with quantum topology. Indeed, it can host exotic fractionalized excitations, such as charge-neutral spinons and Majorana fermions, which can be exploited for fault-tolerant quantum computing [2, 7–10].

The experimental realization of QSLs with exotic topological excitations in archetypical frustrated magnets, such as kagome, triangular, and honeycomb lattices is highly topical in modern condensed matter. In this vein, the triangular lattice (TL) antiferromagnet represents a quintessential model for the experimental realization of QSL states. In

case of isotropic Heisenberg nearest-neighbor interactions, this lattice features a 120° spin-ordered ground state. However, next-neighbor interactions, magnetic anisotropy, or anisotropic exchange interactions can lead to a quantum disordered state in TL representatives. Currently, research efforts have been devoted to 4f rare-earth-based frustrated antiferromagnets, where the synergistic interplay between strong spin-orbit coupling and crystal electric field often leads to a strong exchange anisotropy, thus offering an alternate route to realize the QSL state. This route is based on the spin-orbit coupling which, for Kramers ions, typically implies $J_{\text{eff}} = 1/2$ at low temperature, accompanied by a large magnetic anisotropy due to crystal-field effects [11–21].

Among several QSL scenarios, the intriguing two-dimensional Kitaev model on a bipartite honeycomb lattice with low coordination number offers an exactly solvable model. The frustrated honeycomb magnets, with highly anisotropic bond-dependent ferromagnetic Ising interactions between effective spin-1/2 objects, sustain strong quantum fluctuations. Hence, they provide a natural habitat to stabilize the celebrated Kitaev QSL state, characterized by a spectrum of deconfined fractional excitations, including Majorana fermions, gauge fluxes, and non-abelian statistics.

* pkhuntia@iitm.ac.in

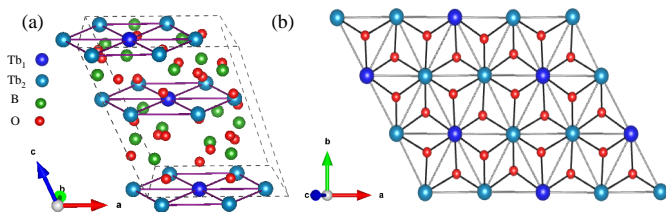


FIG. 1. (a) Schematic diagram of the stuffed honeycomb lattice of Tb^{3+} ions lying in the ab planes of the TbBO_3 monoclinic structure. (b) Top view of one of the stuffed honeycomb planes, showing how Tb^{3+} ions connect to their nearest-neighbors via oxygen ions.

However, defects, stacking faults, and extra perturbing terms in the spin Hamiltonian put a strong constraint to the experimental realization of the elusive Kitaev QSL [22–27]. Strikingly, the highly entangled QSL state can host non-trivial edge states, such as the quantized Hall effect (akin to that observed in two-dimensional electronic systems, including graphene), that offers a promising ground for future quantum technologies [28–30].

Honeycomb magnets containing lanthanides achieve their bond-dependent exchange interaction via the strong spin-orbit driven anisotropy of the $4f$ electrons. Indeed, their localized $4f$ orbitals restrict the exchange interaction between the $4f$ magnetic moments to the nearest neighbors. This represents an ideal route to realize unusual quantum states, including the Kitaev QSL with fractionalized quasiparticles [31, 32]. Interestingly, in the quest for an alternative platform for QSL, theoretical studies have shown that a “stuffed” honeycomb lattice, comprised of a honeycomb lattice with a superimposed triangular lattice formed by additional magnetic ions at the center of each hexagon, can support exotic quantum phenomena, including Dirac QSL [33–36]. The impact of the center spin in stabilizing the QSL in emergent honeycomb lattices has been subject of significant research attention [37]. A QSL has been proposed to occur in $\text{LiZn}_2\text{Mo}_3\text{O}_8$, a emergent honeycomb lattice, where the center Mo spin behaves as a weakly coupled defect [38]. Moreover, it has been suggested that the stuffed honeycomb lattice may host a partially disordered state induced by zero-point quantum fluctuations [33]. This intriguing state entails the coexistence of a Néel antiferromagnetic order (within the honeycomb subsystem) with short-range ferromagnetically coupled central spins, which remain decoupled from the honeycomb sublattice [33]. In addition, the stuffed honeycomb lattice may provide vital clues on the nature of low-energy excitations in the QSL state. Indeed, its center spin can act as a topological defect, whose response resembles that of Friedel oscillations around charge defects or Kondo clouds around magnetic defects [39–41]. The observation of a $1/3$ -magnetization plateau in a rare-earth based stuffed honeycomb lattice [42] has triggered interest on the possible occurrence of Kitaev interactions [43].

Nevertheless, promising stuffed honeycomb contenders

potential to host QSL and Kitaev physics are scarce. Recently, the rare-earth magnet TbInO_3 has been investigated as a possible candidate of a QSL state in a stuffed honeycomb lattice [30, 44, 45]. It consists of two Tb^{3+} sites: a $2a$ site, hosting nonmagnetic Tb_1 ions, and a $4b$ site, hosting nonmagnetic Tb_2 ions which decorate the honeycomb network. Interestingly, terahertz time-domain spectroscopy, an alternative approach for studying highly entangled states, has revealed the presence of charge carriers in archetypal Mott Insulator TbInO_3 , even at ambient temperature. This unveils that the low energy excitation continuum is decoupled from the crystal field transitions at low temperature and robust against external perturbations [46]. At low temperatures, the magnetic Tb^{3+} ions at $4b$ sites were thought to give rise to a Kitaev spin-liquid state [44]. However, it is unclear if the exchange interactions in TbInO_3 are sufficiently anisotropic to allow for it [35]. In addition, it is debated if a monoclinic system can generate the nearly perfect stuffed honeycomb lattice required for hosting a Dirac spin liquid [35]. Currently, potential Kitaev QSL candidate materials are being explored, with the main contenders being frustrated magnets [47].

In this work, we investigated the ground state of a stuffed honeycomb-like lattice antiferromagnet TbBO_3 by μSR , NMR, and thermodynamic measurements. Our density functional theory + Hubbard U (DFT + U) calculations suggest the presence of a significant spin-orbit driven magnetic anisotropy and a frustrated spin-lattice. The ac susceptibility and specific-heat data down to 50 mK rule out the presence of spin freezing and magnetic phase transitions. The power-law behavior of specific heat below the broad maximum around 5 K is consistent with the theoretical prediction of a gapless QSL ground state with Dirac nodes [35]. Despite the sizable antiferromagnetic interaction between Tb^{3+} moments, μSR experiments detect no signatures of long-range magnetic order or spin-freezing down to 16 mK. The enhanced μSR relaxation rate below 3 K is attributed to the slowing down of spin dynamics on cooling and it levels off below 1 K, typical of QSL candidates, thus suggesting a dynamic ground state. Remarkably, the scaling of the muon-spin relaxation rate with the characteristic energy scale of several spin-liquid candidates, including TbBO_3 , demonstrates a thermally activated behavior. This observation suggests that a common physical mechanism drives the dynamic ground state in all the QSL candidates. Similar to μSR , also NMR experiments do not detect signatures of a magnetic ordering or spin freezing down to 2 K. The broadening of the NMR line width at low temperature implies the development of short-range spin correlations, consistent with specific heat and μSR results. In TbBO_3 , short-range spin correlations and a persistent spin dynamics at temperatures much lower than the characteristic interaction energy scale seem to govern the ground state properties.

The Rietveld refinement of the powder XRD data [see Fig. S1 in supplementary material (SM) [48]] reveals that TbBO_3 crystallizes in the monoclinic $C2/c$ space group.

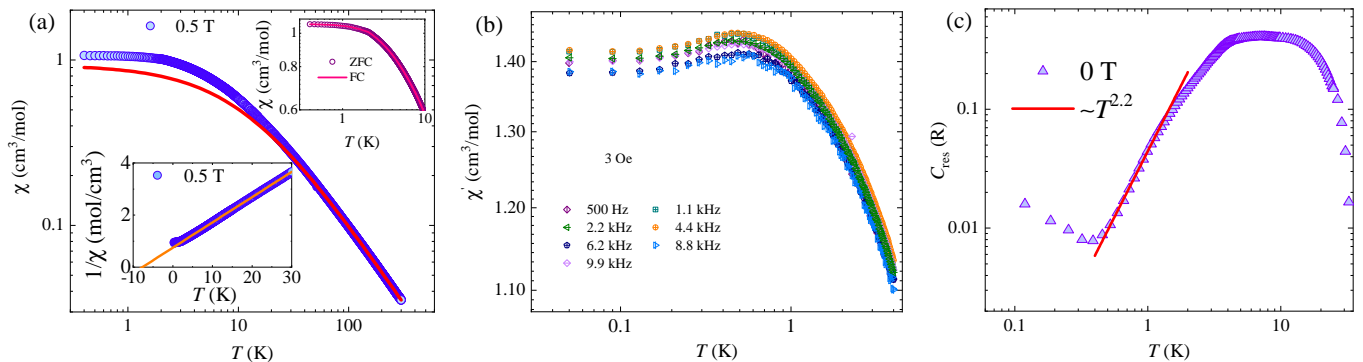


FIG. 2. (a) Temperature dependence of the TbBO_3 magnetic susceptibility collected in a field of 0.5 T and its Curie-Weiss fit (solid red line). The top inset shows the temperature dependence of the zero-field-cooled and field-cooled magnetic susceptibilities. The bottom inset depicts the Curie-Weiss fit to the low-temperature inverse magnetic susceptibility. (b) Temperature dependence of the real part of ac susceptibility at different frequencies down to 50 mK. (c) Temperature dependence of the magnetic specific heat in zero field. Here, the solid line represents a $\sim T^{2.2}$ power-law behavior below 1.4 K.

The obtained lattice parameter and atomic coordinates are presented in SM [48] and confirm the absence of anti-site disorder among the constituent atoms. Figure 1(a) depicts the monoclinic crystal structure of TbBO_3 [49–51], where the Tb^{3+} ions occupy two distinct Wyckoff sites: 4c (Tb_1) and 8f (Tb_2). The nearest-neighbors of the Tb^{3+} ions at the 8f sites are located 3.86 Å apart and form a honeycomb lattice, lying perpendicular to the crystallographic c -axis [Fig. 1(a)]. On the other hand, the Tb^{3+} ions at the 4c sites are located at the center of the hexagons. The overall structure is a “stuffed” honeycomb lattice of Tb^{3+} ions, comprised of a honeycomb lattice with a superimposed triangular lattice, as shown in Fig. 1(a) [49–51]. Figure 1(b) illustrates the intra-planar Tb-O-Tb superexchange paths.

As shown in Fig. 2(a), the absence of any anomalies in the temperature dependence of magnetic susceptibility $\chi(T)$ down to 0.4 K rules out a long-range magnetic order (LRO) of Tb^{3+} moments. Further, the overlapping zero-field cooled and field-cooled $\chi(T)$ data imply that Tb^{3+} spins do not freeze, at least down to 0.4 K [see inset in Fig. 2(a)]. The lack of spin freezing is further supported by low-temperature ac susceptibility measurements performed at different frequencies [see Fig. 2(b)]. The real part of ac susceptibility $\chi'(T)$ exhibits a broad hump around 0.5 K, mostly independent of frequency, similar to other spin-liquid candidates [52–54]. In a spin-glass system, the freezing temperature T_f would have shifted towards higher temperatures with increasing frequency. The absence of such shift here, rules out a spin glass-like behavior of the Tb^{3+} moments down to 50 mK [52]. To estimate the effective magnetic moment μ_{eff} and the Curie-Weiss (CW) temperature θ_{CW} , the inverse magnetic susceptibility data $1/\chi(T)$ were fitted by the CW law $\chi = C/(T - \theta_{\text{CW}})$. Here, the Curie constant C is related to the effective moment by $\mu_{\text{eff}} = \sqrt{8C}\mu_B$, while θ_{CW} represents the energy scale of the magnetic exchange interaction between Tb^{3+} moments. The CW fit to the high-temperature ($T > 50$ K) $1/\chi$ data [red line in Fig. 2(a)] yields an effective

moment of $9.62\mu_B$, close to the theoretical value of $9.72\mu_B$ of the free Tb^{3+} ions (${}^7\text{F}_6$: $S = 3$, $L = 3$). The CW temperature $\theta_{\text{CW}} = -12$ K suggests the presence of low-energy excited crystal electric field (CEF) levels, consistent with our CEF calculations that yield first excited level at 1 meV, which is very close to 12 K, where we have a maximum in C_{res} (see SM) [48]. To obtain a rough estimate of the dominant magnetic interactions between Tb^{3+} moments, the $1/\chi$ data below 25 K were fitted by a CW law, giving $\mu_{\text{eff}} = 9.06\mu_B$, and $\theta_{\text{CW}} = -7.6$ K [50, 55]. The effective moment derived from a CW fit to the low-temperature $\chi(T)$ data is similar to that obtained at high-temperature. This implies a non negligible spin-orbit coupling [50, 56], a scenario is supported also by the CEF and DFT + U calculations which find a significant orbital moment on the Tb-site presented in SM [48]. The obtained negative CW temperature suggests the presence of antiferromagnetic interactions between the Tb^{3+} moments at low-temperature, corroborated also by DFT + U calculations [48].

To obtain further insight into the magnetic correlations and low-energy excitations, we performed specific-heat C_p measurements down to 110 mK. The absence of any λ -type anomaly in C_p suggests that the Tb^{3+} moments do not undergo any LRO, at least down to 110 mK [Fig. 2(c) and Fig. S4 [48]]. Following the subtraction of the lattice contribution (see Fig. S4), the residual specific heat, i.e., $C_{\text{res}}(T) = C_p(T) - C_{\text{lat}}(T)$, is obtained and it is shown in Fig. 2(c). In zero field, C_{res} shows a broad maximum over a wide temperature range, similar to other rare-earth-based magnets [30, 57, 58]. Nonetheless, in case of TbBO_3 , this maximum (ranging from 3 K to 25 K) is attributed to an overlap of the Schottky anomaly (owing to the thermal population of the excited CEF levels) and the short-range spin correlations [30, 56, 59]. Most likely, the broad maximum at ~ 12 K is an effect of the excited CEF levels, broadened by the exchange correlation fields [55]. To confirm the interplay between the magnetic correlations and the excited CEF levels, the C_{res} data were analyzed

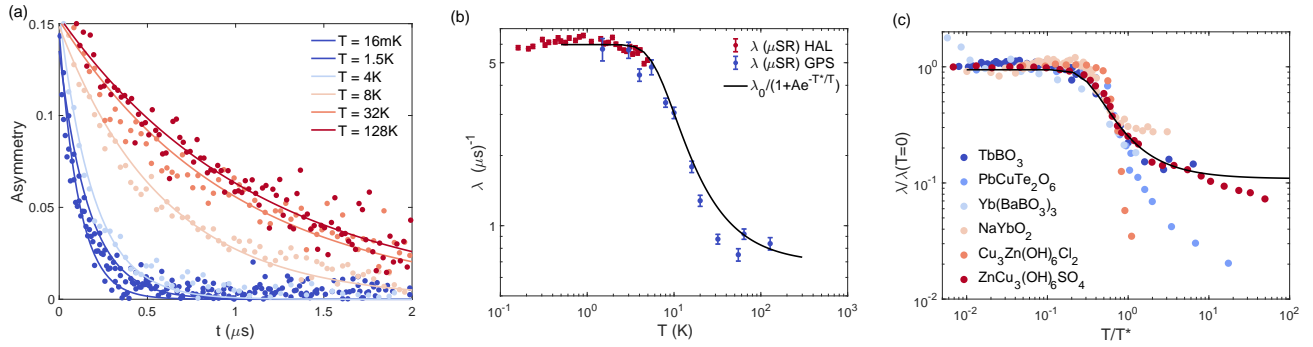


FIG. 3. (a) Time evolution of the μSR asymmetry at representative temperatures. Solid lines represent fits to an exponential function, as described in the text. (b) Temperature dependence of the muon-spin relaxation rate λ . To cover a broad temperature range, the datasets had to be collected at two different μSR spectrometers: HAL and GPS. (c) Temperature-dependent scaling of λ for several potential QSL materials. The solid line in (b) and (c) corresponds to the phenomenological model $\lambda = \lambda_0/[1 + A \exp(-T^*/T)]$, which captures the thermally activated behavior of magnetic moments, with λ_0 and A two constants and $T^* = 20 \pm 6$ K a characteristic energy scale.

using CEF parameters [48]. The solid lines in Fig. S5 demonstrate that, above 10 K, C_{res} is dominated by the excited CEF states while, below 10 K, it is determined mostly by the exchange correlations (see SM) [48]. Indeed, upon lowering the temperature, C_{res} starts to increase, followed by a broad maximum around 5 K reflecting the growth of short-range magnetic correlations, in line with the estimated CW temperature [50, 57, 60, 61]. The thermodynamic signature of short-range magnetic correlations is consistent with the presence of a strong magnetic diffuse scattering below 2 K [61]. On cooling below 1 K, C_{res} follows a $T^{2.2}$ power-law behavior ($0.43 \text{ K} \leq T \leq 1.4 \text{ K}$), in agreement with the theoretically predicted spin-liquid state in a stuffed honeycomb lattice, characterized by gapless excitations [35, 57, 62]. Finally, the increase of C_{res} below 0.4 K is ascribed to the contribution of the nuclear Schottky specific heat from the Tb^{3+} and B^{3+} ions [63, 64].

To ascertain the absence of LRO and spin-freezing, and to unveil unambiguously the spin dynamics in the ground state, we performed zero-field (ZF) μSR measurements on TbBO_3 . As illustrated in Fig. 3(a), a rapid relaxation of muon-spin polarization occurs at early times ($t < 2 \mu\text{s}$), more pronounced at lower temperatures. However, the ZF- μSR asymmetry shows no signatures of oscillation, nor a 1/3 “tail” at long times, thus indicating the absence of internal static magnetic fields at the muon stopping site [44]. To follow the evolution of spin dynamics with temperature, the depolarization function $A(t) = A_0 \exp(-\lambda t)$ was used to describe the ZF- μSR spectra over the entire temperature range, 0.016–128 K. Here, A_0 is the initial asymmetry, while λ represents the muon-spin relaxation rate. Figure 3(b) shows the temperature dependence of λ . As the temperatures decrease, λ exhibits a rising trend, until it reaches a plateau at approximately 5 K, in agreement with the broad maximum observed in the specific heat, C_{res} . This indicates a slowing down of the spin dynamics, attributed to the development of short-range spin correlations [65]. On the other hand, the saturation of λ below 3 K implies a persistent spin dynamics, a characteristic feature of the QSL state [65].

The decrease of λ with temperature in a narrow temperature range ($6 \text{ K} \leq T \leq 30 \text{ K}$, for TbBO_3), is also observed in several other QSL candidate materials, including $\text{PbCuTe}_2\text{O}_6$ [66], $\text{Yb}(\text{BaBO}_3)_3$ [67], NaYbO_2 [65], $\text{Cu}_3\text{Zn}(\text{OH})_6\text{Cl}_2$ [68], and $\text{ZnCu}_3(\text{OH})_6\text{SO}_4$ [69]. To shed light on the low-temperature spin dynamics of these promising QSL materials and to establish a common framework across them, the temperature dependence of λ was fitted using a model of thermally activated behavior of electronic spins [70], where the characteristic energy scale T^* can be interpreted as a measure of the strength of CEF [67]. The normalized μSR relaxation rate data for each of the above QSL materials is plotted in Fig. 3(c). Here, the relaxation is normalized to its $T(0\text{K})$ value, while the temperature is scaled to the characteristic T^* value, at which the μSR relaxation begins to increase on cooling. Interestingly, we observe that, even though the normalized μSR relaxation rates exhibit different temperature dependences above T^* , below it all the QSL candidate materials exhibit the same temperature dependence, in this case corresponding to the same fit curve. This is strong evidence of a generic underlying mechanism being at play at low temperatures in all these promising frustrated magnets [66].

The interplay between competing degrees of freedom in frustrated magnets can lead to intriguing quantum phenomena, requiring the study of the ground-state properties on complementary timescales to identify the underlying mechanisms governing the low-temperature physics. To gain microscopic insight into the static susceptibility and spin dynamics behind the ground state of TbBO_3 , we performed ^{11}B ($I = 3/2$, $\gamma = 13.655 \text{ MHz/T}$) NMR measurements. Figure 4(a) depicts the frequency swept ^{11}B NMR spectra at several temperatures in a fixed magnetic field $\mu_0 H = 3 \text{ T}$. Several conclusions can be drawn from the NMR lineshapes. Firstly, the absence of any quadrupole satellite transitions in the measured frequency range ($\pm 10 \text{ MHz}$ on each side of the main NMR line) suggests that the ^{11}B nucleus undergoes only weak quadrupole interactions. Secondly, despite the presence of two distinct boron crystallographic sites in TbBO_3 ,

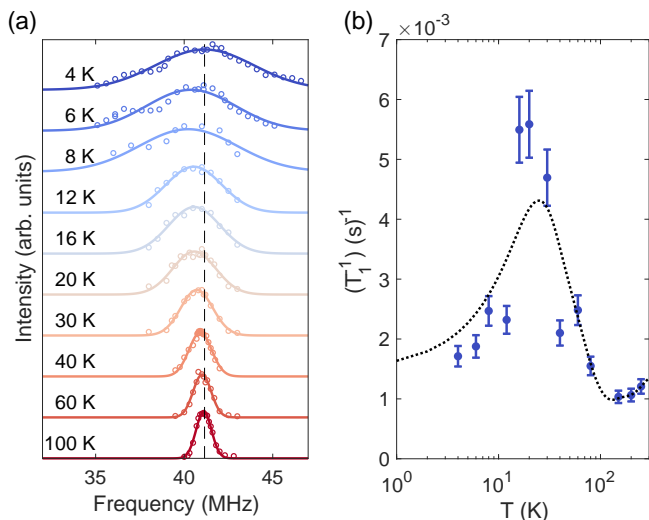


FIG. 4. (a) Frequency-swept ^{11}B NMR spectra measured in a magnetic field of 3 T at various temperatures. Solid lines represent the calculated spectra, with the full width at half maximum as a fit parameter. The reference frequency is shown by the dashed vertical line. (b) ^{11}B NMR spin-lattice relaxation rate (T_1^{-1}) vs. temperature in TbBO_3 . The dashed line is a guide to the eye.

the occurrence of a single broad peak in the ^{11}B NMR spectra indicates equivalent environments for the B nuclei [71]. As we enter the low-temperature regime, we observe that the NMR linewidth broadens significantly, from ~ 1 MHz at 100 K to ~ 8 MHz at 4 K (Fig. S6) [48]. The broadening of the NMR linewidth at low temperatures is a generic feature observed also in other QSL candidates, [66, 71] which reflects the development of short-range spin correlations. The absence of a rectangular NMR lineshape or of peak splitting suggests that long-range magnetic order is absent in TbBO_3 , at least down to 4 K, in agreement with the thermodynamic- and μSR results [72, 73]. Further, the absence of any significant shifts of the boron frequency from its reference value indicates that the hyperfine interaction between the boron nucleus and the magnetic Tb^{3+} ions is of dipolar origin. We now discuss shortly the spin-lattice relaxation rate (T_1^{-1}) in TbBO_3 . T_1^{-1} probes the low-energy spin excitations reflecting the electron-spin fluctuations at the B nucleus site and can be expressed as $\frac{1}{T_1 T} \propto \sum_{\mathbf{q}} |A_{\text{hf}}(\mathbf{q})|^2 \chi''(\mathbf{q}, \omega_0)/\omega_0$, where the summation is over the wave vectors \mathbf{q} within the first Brillouin zone, $A_{\text{hf}}(\mathbf{q})$ is the form factor of the hy-

perfine interactions, and $\chi''(\mathbf{q}, \omega_0)$ represents the dynamic susceptibility at the nuclear Larmor frequency ω_0 [74].

The temperature dependence of T_1^{-1} , derived from the recovery of the longitudinal nuclear magnetization [see Fig. 4(b)], reveals a sharp peak around 20 K. This peak is close to the first excited CEF gap of ~ 12 K obtained from dc susceptibility measurements (Fig. 2) and is consistent also with the μSR characteristic energy scale $T^* = 20 \pm 6$ K (Fig. 3). Furthermore, close to the peak, an NMR “wipeout effect” (see Fig. S6) is observed, resulting in a weak NMR signal and, hence, in large error bars in the T_1^{-1} values. Below 20 K, there is a clear decrease of T_1^{-1} , potentially associated with the slowing down of spins due to the Zeeman splitting of the CEF ground state, with no signatures of LRO [75].

In summary, we investigated the spin-orbit-coupled frustrated stuffed honeycomb antiferromagnet TbBO_3 using thermodynamic-, as well as local-probe techniques. The thermodynamic measurements indicate that the antiferromagnetically coupled Tb^{3+} moments do not exhibit any long-range magnetic order or spin freezing down to 50 mK. Furthermore, the specific heat exhibits a power-law behavior below its broad maximum, supporting the presence of gapless excitations. The CEF calculations reproduce the thermodynamic results reasonably well and suggest that the ground state is well separated from the excited state. DFT calculations suggest the presence of a significant spin-orbit driven magnetic anisotropy. NMR experiments reveal the existence of short-range spin correlations between the Tb^{3+} ions, consistent with the thermodynamic results. The μSR experiments rule out a spin freezing or a magnetic phase transition, but confirm the persistence of spin dynamics down to 16 mK. This implies the emergence of a QSL state within a stuffed honeycomb lattice, thus providing an alternative avenue for investigating the Dirac spin liquids.

P. K. acknowledges support by the Science and Engineering Research Board and the Department of Science and Technology of India through research grants. J. K. thanks M. Barik for the synthesis of a sample batch. M. P. acknowledges funding from the Slovenian Research and Innovation Agency (ARIS) (Project No. J2-2513 and Program No. P1-0125). We acknowledge the allocation of beam time at the Swiss muon source (HAL and GPS μSR spectrometers). S.K.P. acknowledges funding support from a SERB Core Research grant (Grant No. CRG/2023/003063). D.T.A. thanks EPSRC UK (Grant Ref: EP/W00562X/1) for the funding.

- [1] W. Witczak-Krempa, G. Chen, Y. B. Kim, and L. Balents, Correlated quantum phenomena in the strong spin-orbit regime, *Annu. Rev. Condens. Matter Phys.* **5**, 57 (2014).
- [2] L. Balents, Spin liquids in frustrated magnets, *Nature* **464**, 199 (2010).
- [3] S. Jeon, D. Wulferding, Y. Choi, S. Lee, K. Nam, K. H. Kim, M. Lee, T.-H. Jang, J.-H. Park, S. Lee, S. Choi, C. Lee, H. Nojiri, and K.-Y. Choi, One-ninth magnetization plateau stabilized by

spin entanglement in a kagome antiferromagnet, *Nat. Phys.* **20**, 435 (2024).

- [4] C. Broholm, R. J. Cava, S. A. Kivelson, D. G. Nocera, M. R. Norman, and T. Senthil, Quantum spin liquids, *Science* **367**, eaay0668 (2020).
- [5] J. Wen, S.-L. Yu, S. Li, W. Yu, and J.-X. Li, Experimental identification of quantum spin liquids, *npj Quantum Mater.* **4**, 12 (2019).

- [6] P. Khuntia, M. Velazquez, Q. Barthélemy, F. Bert, E. Kermarrec, A. Legros, B. Bernu, L. Messio, A. Zorko, and P. Mendels, Gapless ground state in the archetypal quantum kagome antiferromagnet $\text{ZnCu}_3(\text{OH}_6\text{Cl}_2)$, *Nat. Phys.* **16**, 469 (2020).
- [7] P. W. Anderson, Resonating valence bonds: A new kind of insulator?, *Mater. Res. Bull.* **8**, 153 (1973).
- [8] A. Kitaev, Anyons in an exactly solved model and beyond, *Ann. Phys.* **321**, 2–111 (2006).
- [9] J. Khatua, B. Sana, A. Zorko, M. Gomilšek, K. Sethupathi, M. R. Rao, M. Baenitz, B. Schmidt, and P. Khuntia, Experimental signatures of quantum and topological states in frustrated magnetism, *Phys. Rep.* **1041**, 1 (2023).
- [10] X.-G. Wen, Colloquium: Zoo of quantum-topological phases of matter, *Rev. Mod. Phys.* **89**, 041004 (2017).
- [11] L. Savary and L. Balents, Quantum spin liquids: a review, *Rep. Prog. Phys.* **80**, 016502 (2016).
- [12] B. Bernu, C. Lhuillier, and L. Pierre, Signature of Néel order in exact spectra of quantum antiferromagnets on finite lattices, *Phys. Rev. Lett.* **69**, 2590 (1992).
- [13] Y. Iqbal, W.-J. Hu, R. Thomale, D. Poilblanc, and F. Becca, Spin liquid nature in the Heisenberg $J_1 - J_2$ triangular antiferromagnet, *Phys. Rev. B* **93**, 144411 (2016).
- [14] Z. Zhu and S. R. White, Spin liquid phase of the $s = \frac{1}{2}$ $J_1 - J_2$ Heisenberg model on the triangular lattice, *Phys. Rev. B* **92**, 041105 (2015).
- [15] S. N. Saadatmand and I. P. McCulloch, Symmetry fractionalization in the topological phase of the spin- $\frac{1}{2}$ $J_1 - J_2$ triangular Heisenberg model, *Phys. Rev. B* **94**, 121111 (2016).
- [16] Z. Y. Meng, T. C. Lang, S. Wessel, F. F. Assaad, and A. Muramatsu, Quantum spin liquid emerging in two-dimensional correlated Dirac fermions, *Nature* **464**, 847 (2010).
- [17] M. Baenitz, P. Schlender, J. Sichelschmidt, Y. A. Onykiienko, Z. Zangeneh, K. M. Ranjith, R. Sarkar, L. Hozoi, H. C. Walker, J.-C. Orain, H. Yasuoka, J. van den Brink, H. H. Klauss, D. S. Inosov, and T. Doert, NaYbS_2 : A planar spin- $\frac{1}{2}$ triangular-lattice magnet and putative spin liquid, *Phys. Rev. B* **98**, 220409 (2018).
- [18] M. M. Bordelon, E. Kenney, C. Liu, T. Hogan, L. Posthuma, M. Kavand, Y. Lyu, M. Sherwin, N. P. Butch, C. Brown, M. J. Graf, L. Balents, and S. D. Wilson, Field-tunable quantum disordered ground state in the triangular-lattice antiferromagnet NaYbO_2 , *Nat. Phys.* **15**, 1058 (2019).
- [19] P.-L. Dai, G. Zhang, Y. Xie, C. Duan, Y. Gao, Z. Zhu, E. Feng, Z. Tao, C.-L. Huang, H. Cao, A. Podlesnyak, G. E. Granroth, M. S. Everett, J. C. Neufeind, D. Voneshen, S. Wang, G. Tan, E. Morosan, X. Wang, H.-Q. Lin, L. Shu, G. Chen, Y. Guo, X. Lu, and P. Dai, Spinon fermi surface spin liquid in a triangular lattice antiferromagnet NaYbSe_2 , *Phys. Rev. X* **11**, 021044 (2021).
- [20] A. Kitaev, Anyons in an exactly solved model and beyond, *Ann. Phys.* **321**, 2 (2006).
- [21] G. H. Wannier, Antiferromagnetism. the triangular Ising net, *Phys. Rev.* **79**, 357 (1950).
- [22] J. Nasu, Majorana quasiparticles emergent in Kitaev spin liquid, *Prog. Theor. Exp. Phys.*, ptad115 (2023).
- [23] H. Takagi, T. Takayama, G. Jackeli, G. Khaliullin, and S. E. Nagler, Concept and realization of Kitaev quantum spin liquids, *Nat. Rev. Phys.* **1**, 264 (2019).
- [24] S. Trebst and C. Hickey, Kitaev materials, *Phys. Rep.* **950**, 1 (2022).
- [25] J. Chaloupka, G. Jackeli, and G. Khaliullin, Kitaev-Heisenberg model on a honeycomb lattice: Possible exotic phases in iridium oxides A_2IrO_3 , *Phys. Rev. Lett.* **105**, 027204 (2010).
- [26] K. W. Plumb, J. P. Clancy, L. J. Sandilands, V. V. Shankar, Y. F. Hu, K. S. Burch, H.-Y. Kee, and Y.-J. Kim, $\alpha\text{-RuCl}_3$: A spin-orbit assisted Mott insulator on a honeycomb lattice, *Phys. Rev. B* **90**, 041112 (2014).
- [27] J. A. Sears, L. E. Chern, S. Kim, P. J. Bereciartua, S. Francoual, Y. B. Kim, and Y.-J. Kim, Ferromagnetic Kitaev interaction and the origin of large magnetic anisotropy in $\alpha\text{-RuCl}_3$, *Nat. Phys.* **16**, 837 (2020).
- [28] K. von Klitzing, The quantized Hall effect, *Rev. Mod. Phys.* **58**, 519 (1986).
- [29] Y. Kasahara, T. Ohnishi, Y. Mizukami, O. Tanaka, S. Ma, K. Sugii, N. Kurita, H. Tanaka, J. Nasu, Y. Motome, T. Shibauchi, and Y. Matsuda, Majorana quantization and half-integer thermal quantum Hall effect in a Kitaev spin liquid, *Nature* **559**, 227 (2018).
- [30] J. Kim, X. Wang, F.-T. Huang, Y. Wang, X. Fang, X. Luo, Y. Li, M. Wu, S. Mori, D. Kwok, E. D. Mun, V. S. Zapf, and S.-W. Cheong, Spin liquid state and topological structural defects in hexagonal TbInO_3 , *Phys. Rev. X* **9**, 031005 (2019).
- [31] S.-H. Jang, R. Sano, Y. Kato, and Y. Motome, Computational design of f -electron Kitaev magnets: Honeycomb and hyperhoneycomb compounds A_2PrO_3 , *Phys. Rev. Materials* **4**, 104420 (2020).
- [32] S.-H. Jang, R. Sano, Y. Kato, and Y. Motome, Antiferromagnetic Kitaev interaction in f -electron based honeycomb magnets, *Phys. Rev. B* **99**, 241106 (2019).
- [33] M. G. Gonzalez, F. T. Lisandrini, G. G. Blesio, A. E. Trumper, C. J. Gazza, and L. O. Manuel, Correlated partial disorder in a weakly frustrated quantum antiferromagnet, *Phys. Rev. Lett.* **122**, 017201 (2019).
- [34] J. Sahoo, D. Kochkov, B. K. Clark, and R. Flint, Classical phase diagram of the stuffed honeycomb lattice, *Phys. Rev. B* **98**, 134419 (2018).
- [35] J. Sahoo and R. Flint, Symmetric spin liquids on the stuffed honeycomb lattice, *Phys. Rev. B* **101**, 115103 (2020).
- [36] A. Sil and A. K. Ghosh, Nontrivial topological phases on the stuffed honeycomb lattice, *J. Phys.: Condens. Matter* **32**, 025601 (2019).
- [37] J. P. Sheckelton, J. R. Neilson, D. G. Soltan, and T. M. McQueen, Possible valence-bond condensation in the frustrated cluster magnet $\text{LiZn}_2\text{Mo}_3\text{O}_8$, *Nat. Mater.* **11**, 493 (2012).
- [38] R. Flint and P. A. Lee, Emergent honeycomb lattice in $\text{LiZn}_2\text{Mo}_3\text{O}_8$, *Phys. Rev. Lett.* **111**, 217201 (2013).
- [39] J. Friedel, Xiv. the distribution of electrons round impurities in monovalent metals, *The London, Edinburgh, and Dublin Philosophical Magazine and Journal of Science* **43**, 153 (1952).
- [40] J. Kondo, Resistance Minimum in Dilute Magnetic Alloys, *Prog. Theor. Phys.* **32**, 37 (1964).
- [41] W.-H. Kao, N. B. Perkins, and G. B. Halász, Vacancy spectroscopy of non-abelian Kitaev spin liquids, *Phys. Rev. Lett.* **132**, 136503 (2024).
- [42] N. Yuan, A. Elghandour, W. Hergert, R. Ohlendorf, L. Gries, and R. Klingeler, $1/3$ plateau and $3/5$ discontinuity in the magnetization and the magnetic phase diagram of hexagonal GdInO_3 , *Phys. Rev. B* **108**, 224403 (2023).
- [43] Y. Shangquan, S. Bao, Z.-Y. Dong, N. Xi, Y.-P. Gao, Z. Ma, W. Wang, Z. Qi, S. Zhang, Z. Huang, J. Liao, X. Zhao, B. Zhang, S. Cheng, H. Xu, D. Yu, R. A. Mole, N. Murai, S. Ohira-Kawamura, L. He, J. Hao, Q.-B. Yan, F. Song, W. Li, S.-L. Yu, J.-X. Li, and J. Wen, A one-third magnetization plateau phase as evidence for the Kitaev interaction in a honeycomb-lattice antiferromagnet, *Nat. Phys.* **19**, 1883 (2023).
- [44] L. Clark, G. Sala, D. D. Maharaj, M. B. Stone, K. S. Knight, M. T. F. Telling, X. Wang, X. Xu, J. Kim, Y. Li, S.-W. Cheong, and

- B. D. Gaulin, Two-dimensional spin liquid behaviour in the triangular-honeycomb antiferromagnet TbInO_3 , *Nat. Phys.* **15**, 262 (2019).
- [45] M. Ye, X. Xu, X. Wang, J. Kim, S.-W. Cheong, and G. Blumberg, Crystal-field excitations and vibronic modes in the triangular-lattice spin-liquid candidate TbInO_3 , *Phys. Rev. B* **104**, 085102 (2021).
- [46] T. S. Jung, X. Xu, J. Kim, B. H. Kim, H. J. Shin, Y. J. Choi, E.-G. Moon, S.-W. Cheong, and J. H. Kim, Unconventional room-temperature carriers in the triangular-lattice Mott insulator TbInO_3 , *Nat. Phys.* **19**, 1611 (2023).
- [47] P. Kos and M. Punk, Quantum spin liquid ground states of the Heisenberg-Kitaev model on the triangular lattice, *Phys. Rev. B* **95**, 024421 (2017).
- [48] See supplementary material (SM) for further details on sample characterization, crystal electric field, and DFT calculations.
- [49] J. Lin, D. Sheptyakov, Y. Wang, and P. Allenspach, Structures and phase transition of vaterite-type rare earth orthoborates: a neutron diffraction study, *Chem. Mater.* **16**, 2418 (2004).
- [50] P. Mukherjee, Y. Wu, G. Lampronti, and S. Dutton, Magnetic properties of monoclinic lanthanide orthoborates, LnBO_3 , $\text{Ln} = \text{Gd, Tb, Dy, Ho, Er, Yb}$, *Mater. Res. Bull.* **98**, 173 (2018).
- [51] G. Sala, M. B. Stone, S.-H. Do, K. M. Taddei, Q. Zhang, G. B. Halász, M. D. Lumsden, A. F. May, and A. D. Christianson, Structure and magnetism of the triangular lattice material YbBO_3 , *J. Phys.: Condens. Matter* **35**, 395804 (2023).
- [52] P. M. Sarte, K. Cruz-Kan, B. R. Ortiz, K. H. Hong, M. M. Bordelon, D. Reig-i Plessis, M. Lee, E. S. Choi, M. B. Stone, S. Calder, D. M. Pajerowski, L. Mangin-Thro, Y. Qiu, J. P. Attfield, S. D. Wilson, C. Stock, H. D. Zhou, A. M. Hallas, J. A. M. Paddison, A. A. Aczel, and C. R. Wiebe, Dynamical ground state in the XY pyrochlore $\text{Yb}_2\text{GaSbO}_7$, *npj Quantum Materials* **6**, 42 (2021).
- [53] J. Khatua, S. Bhattacharya, Q. P. Ding, S. Vrtnik, A. M. Strydom, N. P. Butch, H. Luetkens, E. Kermarrec, M. S. R. Rao, A. Zorko, Y. Furukawa, and P. Khuntia, Spin liquid state in a rare-earth hyperkagome lattice, *Phys. Rev. B* **106**, 104404 (2022).
- [54] R. Zhong, S. Guo, G. Xu, Z. Xu, and R. J. Cava, Strong quantum fluctuations in a quantum spin liquid candidate with a co-based triangular lattice, *PNAS* **116**, 14505 (2019).
- [55] M. J. P. Gingras, B. C. den Hertog, M. Faucher, J. S. Gardner, S. R. Dunsiger, L. J. Chang, B. D. Gaulin, N. P. Raju, and J. E. Greedan, Thermodynamic and single-ion properties of Tb^{3+} within the collective paramagnetic-spin liquid state of the frustrated pyrochlore antiferromagnet $\text{Tb}_2\text{Ti}_2\text{O}_7$, *Phys. Rev. B* **62**, 6496 (2000).
- [56] N. D. Kelly, C. Liu, and S. E. Dutton, Structure and magnetism of a new hexagonal polymorph of $\text{Ba}_3\text{Tb}(\text{BO}_3)_3$ with a quasi-2D triangular lattice, *J. Solid State Chem.* **292**, 121640 (2020).
- [57] J. Nagl, D. Flavián, S. Hayashida, K. Y. Povarov, M. Yan, N. Murai, S. Ohira-Kawamura, G. Simutis, T. J. Hicken, H. Luetkens, C. Baines, A. Hauspurg, B. V. Schwarze, F. Husstedt, V. Pomjakushin, T. Fennell, Z. Yan, S. Gvasaliya, and A. Zheludev, Excitation spectrum and spin hamiltonian of the frustrated quantum Ising magnet Pr_3BWO_9 , *Phys. Rev. Res.* **6**, 023267 (2024).
- [58] Z.-F. Ding, Y.-X. Yang, J. Zhang, C. Tan, Z.-H. Zhu, G. Chen, and L. Shu, Possible gapless spin liquid in the rare-earth kagome lattice magnet $\text{Tm}_3\text{Sb}_3\text{Zn}_2\text{O}_{12}$, *Phys. Rev. B* **98**, 174404 (2018).
- [59] H. L. Che, S. J. Li, J. C. Wu, N. Li, S. K. Guang, K. Xia, X. Y. Yue, Y. Y. Wang, X. Zhao, Q. J. Li, and X. F. Sun, Low-temperature specific heat and heat transport of $\text{Tb}_2\text{Ti}_{2-x}\text{Zr}_x\text{O}_7$ single crystals, *Phys. Rev. B* **107**, 054429 (2023).
- [60] T. Fennell, M. Kenzelmann, B. Roessli, M. K. Haas, and R. J. Cava, Power-law spin correlations in the pyrochlore antiferromagnet $\text{Tb}_2\text{Ti}_2\text{O}_7$, *Phys. Rev. Lett.* **109**, 017201 (2012).
- [61] P. Mukherjee, *Investigation of the magnetic and magnetocaloric properties of complex lanthanide oxides*, Ph.D. thesis, Cambridge University (2018).
- [62] Y. Ran, W.-H. Ko, P. A. Lee, and X.-G. Wen, Spontaneous spin ordering of a Dirac spin liquid in a magnetic field, *Phys. Rev. Lett.* **102**, 047205 (2009).
- [63] B. Bleaney and R. W. Hill, Hyperfine structure in terbium metal, *Proc. Phys. Soc.* **78**, 313 (1961).
- [64] R. W. Hill, The specific heats of Tb_2O_3 and Tb_4O_7 between 0.5 and 22 K, *J. Phys. C: Solid State Phys.* **19**, 673 (1986).
- [65] L. Ding, P. Manuel, S. Bachus, F. Grußler, P. Gegenwart, J. Singleton, R. D. Johnson, H. C. Walker, D. T. Adroja, A. D. Hillier, and A. A. Tsirlin, Gapless spin-liquid state in the structurally disorder-free triangular antiferromagnet NaYbO_2 , *Phys. Rev. B* **100**, 144432 (2019).
- [66] P. Khuntia, F. Bert, P. Mendels, B. Koteswararao, A. V. Mahajan, M. Baenitz, F. C. Chou, C. Baines, A. Amato, and Y. Furukawa, Spin liquid state in the 3d frustrated antiferromagnet $\text{PbCuTe}_2\text{O}_6$: NMR and Muon spin relaxation studies, *Phys. Rev. Lett.* **116**, 107203 (2016).
- [67] C. Y. Jiang, Y. X. Yang, Y. X. Gao, Z. T. Wan, Z. H. Zhu, T. Shiroka, C. S. Chen, Q. Wu, X. Li, J. C. Jiao, K. W. Chen, Y. Bao, Z. M. Tian, and L. Shu, Spin excitations in the quantum dipolar magnet $\text{Yb}(\text{BaBO}_3)_3$, *Phys. Rev. B* **106**, 014409 (2022).
- [68] B. Fåk, E. Kermarrec, L. Messio, B. Bernu, C. Lhuillier, F. Bert, P. Mendels, B. Koteswararao, F. Bouquet, J. Ollivier, A. D. Hillier, A. Amato, R. H. Colman, and A. S. Wills, Kagome quantum spin liquid with competing interactions, *Phys. Rev. Lett.* **109**, 037208 (2012).
- [69] M. Gomilšek, M. Klanjšek, M. Pregelj, F. C. Coomer, H. Luetkens, O. Zaharko, T. Fennell, Y. Li, Q. M. Zhang, and A. Zorko, Instabilities of spin-liquid states in a quantum kagome antiferromagnet, *Phys. Rev. B* **93**, 060405 (2016).
- [70] P. J. Baker, S. J. Blundell, F. L. Pratt, T. Lancaster, M. L. Brooks, W. Hayes, M. Isobe, Y. Ueda, M. Hoinkis, M. Sing, M. Klemm, S. Horn, and R. Claessen, Muon spin relaxation measurements on the dimerized spin 1/2 chains $\text{NaTiSi}_2\text{O}_6$ and TiOCl , *Phys. Rev. B* **75**, 094404 (2007).
- [71] K. Y. Zeng, L. Ma, Y. X. Gao, Z. M. Tian, L. S. Ling, and L. Pi, Nmr study of the spin excitations in the frustrated antiferromagnet $\text{Yb}(\text{BaBO}_3)_3$ with a triangular lattice, *Phys. Rev. B* **102**, 045149 (2020).
- [72] Y. Yamada and A. Sakata, An analysis method of antiferromagnetic powder patterns in spin-echo nmr under external fields, *J. Phys. Soc. Jpn.* **55**, 1751 (1986).
- [73] A. C. Shockley, F. Bert, J.-C. Orain, Y. Okamoto, and P. Mendels, Frozen state and spin liquid physics in $\text{Na}_4\text{Ir}_3\text{O}_8$: An NMR study, *Phys. Rev. Lett.* **115**, 047201 (2015).
- [74] A. Abragam, *The Principles of Nuclear Magnetism* (Clarendon Press, Oxford, 1978).
- [75] K. Y. Zeng, F. Y. Song, Z. M. Tian, Q. Chen, S. Wang, B. Liu, S. Li, L. S. Ling, W. Tong, L. Ma, and L. Pi, Local evidence for collective spin excitations in the distorted kagome antiferromagnet Pr_3BWO_9 , *Phys. Rev. B* **104**, 155150 (2021).